Quantum transport quality of a processed undoped Ge/SiGe heterostructure

Yi-Xin Li [1,*] Zhenzhen Kong [2,3,*] Shimin Hou [1] Guilei Wang [2,4,†] and Shaoyun Huang [1,‡]

[1]*Beijing Key Laboratory of Quantum Devices, Key Laboratory for the Physics and Chemistry of Nanodevices, Peking University, Beijing 100871, People's Republic of China*

[2]*Integrated Circuit Advanced Process R&D Center, Institute of Microelectronics, Chinese Academy of Sciences, Beijing 100029, People's Republic of China*

[3]*School of Integrated Circuits, University of Chinese Academy of Sciences, Beijing 100049, People's Republic of China*

[4]*Hefei National Laboratory, Hefei 230088, People's Republic of China and Beijing Superstring Academy of Memory Technology, Beijing 100176, People's Republic of China*

(Received 9 January 2023; revised 12 June 2023; accepted 13 June 2023; published 7 July 2023)

A degraded mobility of $5.2 \times 10^5\,\mathrm{cm^2\,V^{-1}\,s^{-1}}$ but a long quantum scattering time of 2.3 ps at the hole density of $2.25 \times 10^{11}\,\mathrm{cm^{-2}}$ were obtained from a two-dimensional hole gas in a processed undoped Ge/SiGe heterostructure Hall-bar field-effect device. The heterostructure was grown by the reduced pressure chemical vapor deposition method and the device fabrications were compatible with well-established semiconductor technology. The percolation density of $0.69 \times 10^{11}\,\mathrm{cm^{-2}}$ indicated a very low disorder potential landscape experienced by holes in the strained Ge quantum well. In addition to integer quantum Hall effects (IQHEs) of consecutive filling factors from $\nu = 8$ down to 1, we also observed the quantum states at filling factors between $\nu = 1$ and 2, and between $\nu = 2$ and 3 at 1.71 K. The observation of quantum Hall effects at the inferior mobility confirmed the mobility/quality dichotomy in the ultraclean undoped Ge/SiGe heterostructure. The study explicitly indicated that the device fabrication process likely compromised the transport mobility, whereas the quantum quality was less influenced, and established the heterostructure as an ideal platform for quantum device implementations.

DOI: 10.1103/PhysRevB.108.045303

I. INTRODUCTION

Benefiting from high mobility, light hole effective mass, and inherent strong spin-orbit interaction, confined two-dimensional hole gas (2DHG) in the strained Ge quantum well (QW) has been emerging as a pioneer semiconductor platform that brings together low disorder and electrical tunability for scalable gate-based quantum devices [1–3]. In recent years, we have witnessed a benchmarking on mobility of 2DHG in undoped Ge/SiGe heterostructures, which drastically reduced remote scattering centers and suppressed tunneling from the Ge QW. The hole mobility of the undoped Ge/SiGe at low temperature exceeded $1 \times 10^6\,\mathrm{cm^2\,V^{-1}\,s^{-1}}$ at the beginning of 2022 [4] and reached the higher mobility over $2 \times 10^6\,\mathrm{cm^2\,V^{-1}\,s^{-1}}$ in 2023 in an updated study [5]. The high mobility, in general, suggested high material quality and built a foundation of exploring exotic quantum phenomena [6,7]. The quantum Hall states of integer and fractional filling factors have been observed at low temperature under accessible magnetic field strength in the ultrahigh mobility featuring undoped Ge QW [4,5]. Empirically, with the lower mobility of $\sim 5 \times 10^5\,\mathrm{cm^2\,V^{-1}\,s^{-1}}$ in earlier studies [8,9], only integer quantum Hall effect (IQHE) has manifested with the absence of fractional filling factors. In a recent study, however, the signatures of $\nu = 5/3$ filling factor states have been demonstrated in the undoped Ge/SiGe heterostructure at the even lower mobility of $\sim 2 \times 10^5\,\mathrm{cm^2\,V^{-1}\,s^{-1}}$ [10]. The observation of quantum Hall effects likely was not necessarily related to the ultrahigh mobility.

Depending on the specific transport property of interest, mobility and quality could be determined by different aspects of the underlying disorder distribution. For modulation-doped GaAs/AlGaAs heterostructure counterparts, the mobility/quality dichotomy has been both theoretically and experimentally demonstrated in high-mobility samples since these systems were dominated by long-range Coulomb potential from both near and far random, charged impurity centers [11,12]. Mobility scattering time (i.e., transport lifetime) and quantum scattering time (i.e., quantum lifetime) are two essential timescales in understanding the transport property of the 2DHG system. The mobility scattering time τ_t is dominantly sensitive to large-angle scattering, which mainly originates from the charged impurities near or residing in the conduction channel. τ_t, therefore, relates to conductivity, and can be obtained from *mobility* (μ) by Boltzmann transport theory; $\mu = e\tau_t/m^*$ (m^* is the carrier effective mass). On the other hand, the quantum scattering time τ_q is sensitive to entire scattering events as a measure of the lifetime of a single particle in a momentum eigenstate. τ_q, thus, is responsible for the single-particle level broadening $\Gamma = \hbar/2\tau_q$ of the momentum eigenstate and can be determined experimentally from the amplitude of Shubnikov–de Haas oscillation. In principle, the mobility/quality dichotomy could occur because τ_t and τ_q are

*These authors contributed equally to this work.
‡syhuang@pku.edu.cn
†guilei.wang@bjsamt.org.cn

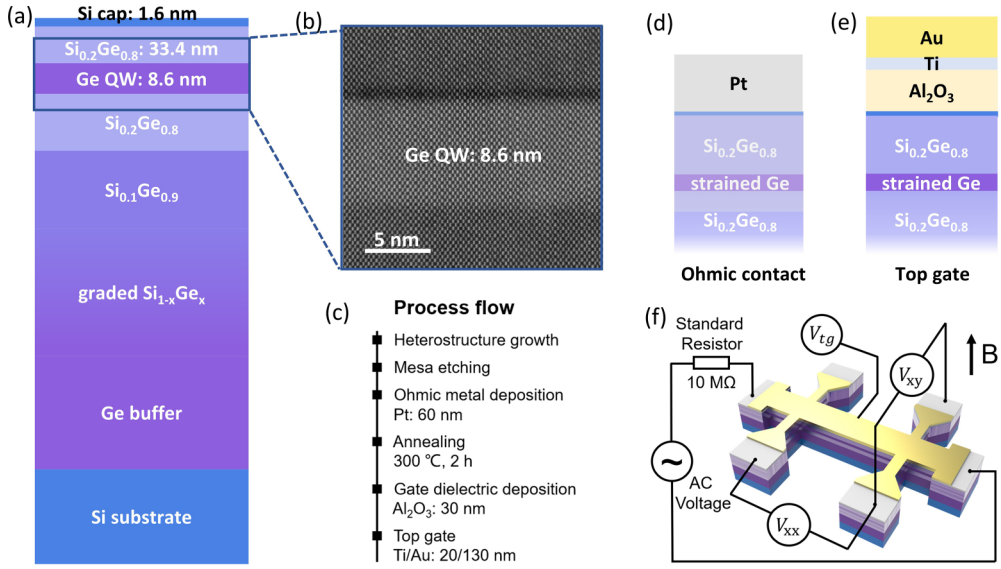

FIG. 1. (a) Layer schematic of the as-grown Ge/SiGe heterostructure. (b) TEM of the strained Ge quantum well, which was positioned between two strain-relaxed layers of $Si_{0.2}Ge_{0.8}$ at a depth of 33.6 nm. (c) Fabrication process flow of Ge/SiGe Hall-bar devices. (d) Schematics of cross section of Ohmic contacts. (e) Schematics of cross section of top gate. (f) Schematics of the Hall-bar field-effect device and the measurement setup.

independent functions of the disorder distribution in ultrahigh-mobility systems [10–13]. To be specific, the mobility is not always a comprehensive indicator of the quality with respect to a certain transport property (e.g., quantum Hall states of fractional filling factors). Alternatively, τ_q is a much more informative indicator of the *quality* for the narrow gap protected fragile quantum states. As the carrier mobility is usually considerably degraded from as-grown structures after device processing, it is desirable to clarify if the mobility/quality dichotomy occurs in the undoped Ge/SiGe heterostructure so that high quantum quality is still expectable in the processed device.

In the present study, we demonstrated that the mobility/quality dichotomy happened in the undoped Ge/SiGe heterostructure and favored quantum implementations in the processed device from as-grown heterostructures. The undoped Ge/SiGe heterostructure was prepared by the reduced pressure chemical vapor deposition (RPCVD) method. The field-effect Hall-bar devices were fabricated via the processes compatible with well-established semiconductor technology for magnetotransport characterization. Despite a degraded hole mobility of $5.2 \times 10^5\ cm^2\ V^{-1}\ s^{-1}$, we observed clear IQHE and the quantum Hall states of filling factors between $\nu = 1$ and 2, and between $\nu = 2$ and 3 at 1.71 K at hole density as low as $1.54 \times 10^{11}\ cm^{-2}$ with a long quantum scattering time τ_q up to 1.2 ps. The study explicitly indicated that the device fabrication process likely compromised the carrier mobility, whereas the quantum quality could be less influenced, so that quantum device implementations less influenced too.

II. EXPERIMENTS

The Ge/SiGe heterostructure, as shown in Fig. 1(a), was grown by the reduced pressure chemical vapor deposition (RPCVD) method. Germane (GeH_4) diluted in H_2 and dichlorosilane (SiH_2Cl_2, DCS) were used as precursors without involving dopant sources. The undoped structure could eliminate the disorder caused by dopant atoms, which were the main sources of scattering. The Ge/SiGe heterostructure contained 1.7 μm Ge as a virtual substrate (Ge VS), which used a two-step method including a low temperature of 450° C and a cap of layers at 650° C. A 750 nm reverse grading layer with Ge contents changed from a pure Ge layer to a $Si_{0.1}Ge_{0.9}$ layer, and a 200 nm $Si_{0.1}Ge_{0.9}$ step layer was grown at 800° C with a thinner reverse gradient buffer to obtain a better material quality. The active layer contained an 8.6 nm thick Ge QW and two $Si_{0.2}Ge_{0.8}$ barrier layers. A 360 nm $Si_{0.2}Ge_{0.8}$ under a barrier layer was grown at 650° C. The thickness of the upper $Si_{0.2}Ge_{0.8}$ barrier layer was 33.6 nm. Before growth of this layer, the surface of the Ge QW layer was treated by DCS to form a sharp interface between Ge and SiGe. As shown in Fig. 1(b), the transmission-electron microscope (TEM) image of the active layers showed a clear interface between the 8.6 nm thick Ge QW and each $Si_{0.2}Ge_{0.8}$ barrier layer. The band-edge alignment between compressively strained Ge and relaxed $Si_{0.2}Ge_{0.8}$ layers formed a *type-I* band energy landscape [14], allowing hole confinement in the strained Ge QW. The shallow upper barrier layer with a thickness of 33.6 nm was designed for the balance between the efficient gate control of the carriers in the Ge QW [15] and the suppression of surface tunneling from the strained Ge QW. A subsequent 1.6 nm thick Si cap layer aimed to protect the underneath SiGe surface against natural oxidation and damage during the device fabrications. The Ge QW, the upper barrier layer, and the Si cap were grown at 500° C.

Hall bar shaped field-effect devices were fabricated aligned to the ⟨110⟩ crystallographic orientation. Due to the face-centered cubic structure of Ge lattices, the atoms distribute most closely in the ⟨110⟩ crystallographic orientation. The strain is most likely to release gradually and regularly through dislocation slip in the direction of the closest atomic

arrangement, avoiding penetrating threading dislocation that leads to dislocation scattering in Ge QW. The fabrication processes shown in Fig. 1(c) were compatible with well-established semiconductor manufacturing technology (see the Supplemental Material, Fig. S1 [16] and, in turn, unavoidably introduced damages and disorders in the device. As schematically displayed in Fig. 1(d), the vacuum thermal annealing assisted platinum (Pt) to penetrate through the upper SiGe barrier and diffuse into the quantum well, realizing Ohmic contacts between the source/drain electrodes and the quantum well due to negligibly low Pt germanosilicide Schottky barrier height for holes [17]. Figure 1(e) illustrates cross-sectional schematics of the top gate, which was made of a 30 nm thick gate dielectric of Al_2O_3 and a metal Ti/Au bilayer. Considerable charged impurities presented at the interface between the Al_2O_3 thin film and the Si cap layer.

Figure 1(f) shows the schematics of the Hall-bar field-effect device and the magnetotransport measurement setup. The Hall-bar device was measured in a Quantum Design Physical Property Measurement System (PPMS). In this study, unless specified differently, we performed the measurements at 1.71 K to stabilize the temperature during a sweeping magnetic field. Instead of nonlinear magnetotransport measurement [18,19], we performed linear magnetotransport measurements as functions of temperature and hole density. The external magnetic field was applied perpendicular to the quantum well. An alternating current with a low frequency of 17 Hz and consistent amplitude of 40 nA was applied between source and drain. Two lock-in amplifiers were used to record the transverse voltage V_{xy} and longitudinal voltage V_{xx} simultaneously. The width W and the length L of the measured region were 80 and 270 μm, respectively. The longitudinal resistivity ρ_{xx} was obtained by $\rho_{xx} = (W/L)(V_{xx}/I)$, and the transverse resistivity (also called Hall resistivity) ρ_{xy} was defined by $\rho_{xy} = V_{xy}/I$. A negative dc voltage V_{tg} was applied on the top gate to accumulate 2DHG in the Ge QW in a controlled manner [20]. The measured 2DHG hole density p_{2D} was tunable from 1.21×10^{11} to 2.40×10^{11} cm^{-2} (see the Supplemental Material, Fig. S2 [16]). The percolation density was extrapolated to 0.69×10^{11} cm^{-2} (see the Supplemental Material, Fig. S3 [16]); also see [21,22], indicating a very low disorder potential landscape experienced by holes in the strained Ge QW.

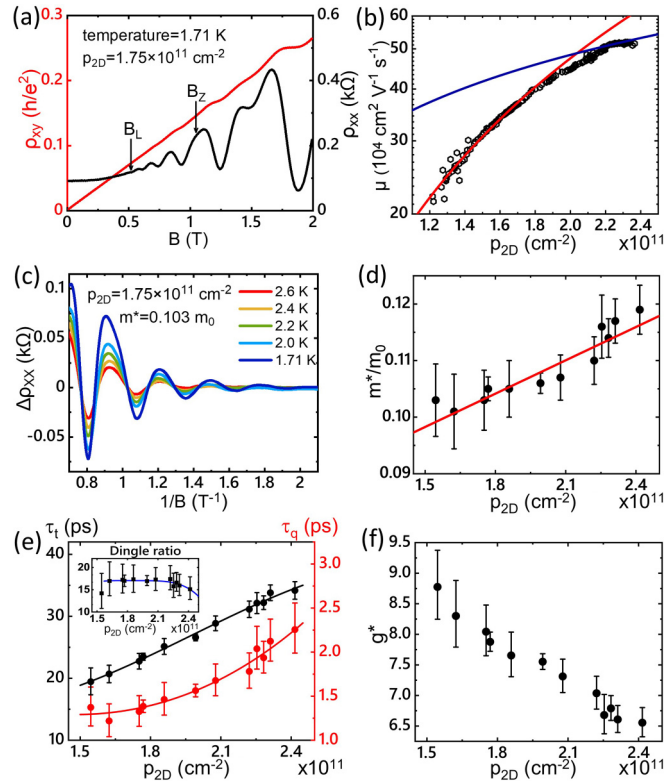

FIG. 2. Transport properties at the temperature of 1.71 K. (a) Transverse Hall resistance ρ_{xy} (red) and longitudinal resistivity ρ_{xx} (black) measured at a hole density of 1.75×10^{11} cm^{-2} as a function of perpendicular magnetic field B ($0<B<2$ T). (b) Mobility μ vs hole density p_{2D}. The red line is the fit to $\mu \propto p_{2D}^{3/2}$, and the blue line is the fit to $\mu \propto p_{2D}^{1/2}$. (c) Temperature dependencies of Shubnikov–de Haas oscillation amplitudes $\Delta\rho_{xx}$ as a function of $1/B$ at a hole density of 1.75×10^{11} cm^{-2}. (d) Effective mass m^* vs p_{2D}; the red line is a linear fit. (e) Mobility scattering time τ_t (black) and quantum scattering time τ_q (red) vs p_{2D}. The inset is the Dingle ratio τ_t/τ_q vs hole density p_{2D}. The blue line is a guide to the eye. (f) Effective Landau g factor g^* vs hole density p_{2D}.

III. RESULTS

A. Magnetotransport properties

Figure 2(a) provides representative Hall measurement data, in which the transverse (Hall) resistance ρ_{xy} is in red and longitudinal resistivity ρ_{xx} is in black, at low magnetic fields. The ρ_{xy} increased linearly with magnetic field B up to 0.5 T. The hole density p_{2D} of 1.75×10^{11} cm^{-2} was, thus, extracted from the Hall resistivity by the Hall coefficient in the relation of $\rho_{xy} = B/ep_{2D}$ within the low magnetic field region ($B<0.1$ T). As the magnetic field further increased, the onset of Shubnikov–de Haas (SdH) oscillations was visible at a critical magnetic field strength of B_L with a filling factor of $\nu = 14$, arising from the fact that the Landau level separation was enhanced wider than the Zeeman energy splitting plus the Landau level broadening. The ρ_{xx} manifested a regular sequence of SdH peaks and the oscillation amplitudes rose with increasing B. When the magnetic field was made stronger, the spin polarization due to Zeeman spin splitting was recognized at another critical magnetic field strength of B_Z with a filling factor of $\nu = 7$. The observation of SdH oscillations preliminarily attested a clean two-dimensional transport system, and allowed the extraction of effective mass m^*, quantum scattering time τ_q, and effective g factor g^*.

Figure 2(b) shows the hole mobility μ as a function of hole density. The μ is obtained from 2D Drude model by $\mu = 1/(ep_{2D}\rho_{xx})$. In the relatively low hole density region, μ increased rapidly due to the improved screening of scattering from remote charged impurities. In the higher hole density region, μ saturated at a maximum of 5.2×10^5 cm^2 V^{-1} s^{-1}, limited by the Ge-SiGe interface roughness, at a hole density of 2.25×10^{11} cm^{-2}. The mean free path (l) of the hole was deduced to be as long as 4.1μm (see the Supplemental Material, Fig. S4 [16]), far greater than the thickness of Ge QW but significantly less than the size of the Hall bar. Scattering

from charge centers determined the 2D transport properties and could be derived from many sources in the processed heterostructure: background charged impurities very close to or inside the Ge quantum well, short-range interface roughness at the Ge-SiGe interfaces, short-range alloy disorder in the insulating SiGe layers, remote charged impurities at the interface between the cap-Si layer and Al_2O_3 thin-film, etc. As for the interface roughness, the mobility is expected to drop with increasing hole density. Such expectation is clearly contrary to the observation shown in Fig. 2(b). The alloy dislocation dominates the 2DHG system at high carrier density when the mobility is greater than 10^7 cm^2 V^{-1} s^{-1} [23], which is two orders of magnitude higher than that of our 2DHG. In this undoped system, therefore, we limited our analysis in the following two kinds of scattering sources: the remote charged impurities and the background charged impurities [11]. The remote charged impurities can be efficiently screened from the Ge QW by hole accumulation therein and, therefore, dominate the transport at low hole density. In contrast, the background charged impurities very close to or inside the Ge quantum well dominate at high hole density. The mobility μ presents distinct power law dependencies of p_{2D} upon the specific scattering mechanism [23]. In the case that the remote charged impurities scattering dominates, the μ follows the power law by $\mu \propto p_{2D}^{3/2}$ and is described by the following [23]:

$$\mu_{\text{remote}} = \frac{16\sqrt{\pi g_v g_s} e h_{\text{eff}}^3}{\hbar N_R} p_{2D}^{3/2}. \tag{1}$$

Otherwise, in the case that the background charged impurities scattering dominates, μ follows the power law by $\mu \propto p_{2D}^{1/2}$ and is described by the following [23]:

$$\mu_{\text{background}} = \frac{(g_v g_s)^{3/2} e}{4\sqrt{\pi}\hbar(N_B/h_{\text{QW}})} p_{2D}^{1/2}. \tag{2}$$

N_R and N_B are the effective density of the remote charged impurities and the background charged impurities, respectively. Accounting for the fact that the remote charged impurities are mostly located at the Al_2O_3-Si interface [24], we set the effective distance h_{eff} between the remote charged impurities and 2DHG to be 39.5 nm, which was the distance between the center of the Ge QW and the bottom of the metal gate. h_{QW} was the thickness of the Ge QW, 8.6 nm. Valley degeneracy g_v is unity and spin degeneracy g_s is double in both equations. The fit to Eq. (1) was applied when p_{2D} was less than 1.80×10^{11} cm^{-2} and indicated in red. The density of the remote charged impurities N_R was thus extracted at 8.7×10^{11} cm^{-2}. When the hole density was in the range from 2.15×10^{11} to 2.30×10^{11} cm^{-2}, the fit to Eq. (2) was applied and displayed in blue. The effective density of the background charged impurities N_B was extracted at 7.9×10^8 cm^{-2}, which was much lower than N_R by three orders of magnitude and attested to very low levels of disorder in the Ge QW. There was, therefore, plenty of room to reduce total scattering by means of improvement on the remote charged impurities at the Al_2O_3-Si interface.

Figure 2(c) shows the temperature dependencies of SdH oscillation amplitudes $\Delta\rho_{xx}$ after baseline subtraction as a function of an inverse magnetic field scale, $1/B$. The SdH oscillation was in single periodicity with respect to $1/B$. The oscillation amplitudes $\Delta\rho_{xx}$ were significantly suppressed with increasing temperature and can be described by the Lifshitz-Kosevich (LK) formula as follows [25],

$$\Delta\rho_{xx} = 4\rho_0 X(T)\exp(-\pi/\omega_c\tau_q), \tag{3}$$

where $X(T)$ is a temperature-damping factor in the expression of $(\frac{2\pi^2 k_B T}{\hbar\omega_c})/\sinh(\frac{2\pi^2 k_B T}{\hbar\omega_c})$, ρ_0 the longitudinal resistivity at zero field, $\omega_c = eB/m^*$ the cyclotron frequency, k_B the Boltzmann constant, and $\hbar$ the reduced Planck constant. Consequently, the effective mass m^* and quantum scattering time τ_q can be extracted by fitting oscillation peaks or valleys located below the spin splitting threshold (see the Supplemental Material, Fig. S5 [16]; also see [25–30]).

Figure 2(d) demonstrates the normalized effective mass m^* with respect to the free electron mass m_0 as a function of hole density. The m^* slightly increased from $0.101m_0$ to $0.119m_0$ when the hole density was populated from 1.54×10^{11} to 2.40×10^{11} cm^{-2}. The red line was a linear fit, which implied the valence band nonparabolicity (see the Supplemental Material, Fig. S6 [16]; also see [31,32]) arising from the interaction between energy spaced heavy and light hole bands in Ge/SiGe heterostructures [33,34]. The extrapolation of the linear fit at the hole density of zero (the topmost heavy hole subband) allowed m^* to arrive at $0.069 \pm 0.005\ m_0$. The extrapolated hole effective mass at zero hole density was close to but slightly larger than that from the theoretical prediction of $\sim 0.05m_0$ by using density functional theory [33]. The discrepancy could be attributed to the specific strain distribution and the detailed roughness at the interface between the Ge QW and the upper $Si_{0.2}Ge_{0.8}$ barrier layer [4,5,29,34]. Nevertheless, the light effective mass gives rise to large orbital-level spacing in quantum dots for the implementation of spin qubits and is, therefore, preferable to relax lithographic-fabrication scales.

Figure 2(e) shows the two crucial timescales, mobility scattering time τ_t, and quantum scattering time τ_q, as a function of hole density. Herein, τ_t was extracted from the Boltzmann transport theory by $\mu = e\tau_t/m^*$, and increased from 19 to 34 ps as the hole density was populated from 1.54×10^{11} to 2.40×10^{11} cm^{-2}. The τ_q was extracted based on the m^* from the fit to Eq. (3) and varied from 1.2 to 2.3 ps, which was longer than that of the early studies where comparable mobility was reported [8,9]. Overall, τ_q was proportional to the accessible hole density as the increased screening significantly reduced the scattering events from charged impurities [35]. The long τ_q guarantees a small level broadening and the high quality for quantum implementations [2,3,36,37]. The inset of Fig. 2(e) shows the Dingle ratio $\alpha = \tau_t/\tau_q$ as a function of the hole density. As p_{2D} was populated from 1.75×10^{11} to 2.40×10^{11} cm^{-2}, the Dingle ratio lowered from 17.4 to 15.1, but was still significantly greater than unity. The relatively small ratio compared with early studies [5,8,9] could derive from the fact that the distribution of impurities at the Al_2O_3-Si interface was more concentrated toward the location of the 2DHG. As p_{2D} was populated, the reduced Dingle ratio implied a crossover from remote impurity scattering limited transport to background impurity scattering limited transport and pronounced large-angle scattering in the entire scattering events. Such a situation was reported in Si QW of undoped Si/SiGe heterostructures as well [38,39].

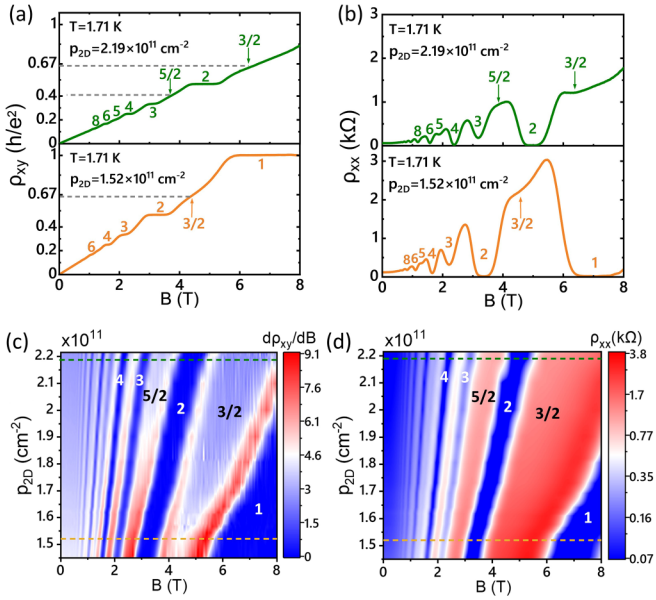

FIG. 3. Quantum Hall effects and Landau fan diagrams. (a) ρ_{xy} and (b) ρ_{xx} are shown as a function of B at two distinct hole densities. (c), (d) Landau fan diagram of derivative $d\rho_{xy}/dB$ and ρ_{xx}, respectively, as functions of p_{2D} and B at a temperature of 1.71 K. The dashed horizontal lines are line cuts at $p_{2D} = 2.19 \times 10^{11}$ cm^{-2} (in green) and $p_{2D} = 1.52 \times 10^{11}$cm^{-2} (in orange) and correspond to ρ_{xy} and ρ_{xx} in (a), (b), respectively.

The out of plane effective Landau g factor g^*, which is an indicator of the strength of spin-orbit interactions, is shown in Fig. 2(f) as a function of hole density. In principle, a large g^* is an ingredient in realizing full-electric manipulations of spin degree of freedom and topological transitions of narrow band semiconductors [40–42]. The g^* was extracted from the critical magnetic field of SdH oscillation as follows [8]:

$$g^* = \frac{2m_0}{m^*} \frac{1}{1 + \sqrt{B_S/B_L}}. \tag{4}$$

The obtained g^* was inversely proportional to the hole density p_{2D}, decreasing from 8.8 to 6.6 with p_{2D} populated from 1.54×10^{11} to 2.40×10^{11} cm^{-2}. The hole density dependent g^* derived from the mixture of the light and the heavy hole states due to the nonparabolicity of the valence band [42,43].

B. Quantum Hall effects

Figure 3(a) provides the transverse (Hall) resistance ρ_{xy} in a wide range of magnetic fields at two distinct hole densities, and Fig. 3(b) provides the corresponding longitudinal resistivity ρ_{xx}. Quantum Hall plateaus of consecutive integer filling factors ν from 1 up to 8 were clearly seen in the ρ_{xy} traces at the hole densities of 2.19×10^{11} cm^{-2} (in green) and 1.52×10^{11}cm^{-2} (in orange). The ρ_{xx} manifested a minimum for each Quantum Hall plateau. Importantly, the ρ_{xx} minima corresponding to the filling factors of 6, 4, and 2 reached clear zeros, ruling out parallel conduction paths and indicating that the transport involved a single high-mobility subband of the heavy hole fundamental state in the Ge QW. Remarkably, there were plateaulike structures in the transverse (Hall) resistance ρ_{xy} at the filling factors between $\nu = 1$ and 2, and between $\nu = 2$ and 3. The corresponding ρ_{xx} also manifested a valleylike minimum to the quantum states at these filling factors. The quantum states at the noninteger filling factors were recognizable at $p_{2D} = 2.19 \times 10^{11}$ cm^{-2}, whereas they were partially invisible at the less populated $p_{2D} = 1.52 \times 10^{11}$ cm^{-2}.

In order to visualize the quantum Hall effect, Landau fan diagrams are shown in Figs. 3(c) and 3(d). For clarity, the derivative $d\rho_{xy}/dB$ rather than ρ_{xy} is displayed in Fig. 3(c), in which the quantum plateau is indicated by a blue stripe and the transition between neighboring plateaus is indicated by a red stripe. As shown in Fig. 3(d), the valleys and peaks of ρ_{xx} are represented by the blue stripes and the red stripes, respectively. The integer filling factors in the fan diagrams fanned out toward a higher magnetic field and hole density at a slope of ν/φ_0 ($\varphi_0 = h/e$ is the magnetic flux quantum), which agreed with the single-subband model. At the filling factors between $\nu = 1$ and 2, and between $\nu = 2$ and 3, the corresponding quantum Hall states developed into plateaulike structures at plausible filling factors $\nu = 5/2$ and $\nu = 3/2$, highlighting the density-dependent evolution of the fractional filling factors. As the hole density decreased, the quantum states at the fractional filling factors gradually vanished, and the minima of ρ_{xx} associated with the filling factors became shallow. The evolution agreed well with the change of quantum scattering time with regard to the hole density, as shown in Fig. 2(e). In the present study, the Landau fan diagrams with the fine structures of quantum Hall states were obtained at a relatively high temperature (1.71 K) compared to the early studies [4,5]. The quantum states at plausible filling factors $\nu = 5/2$ and $\nu = 3/2$ were expected to be much more remarkable at lower temperatures and had been well addressed at a slightly high hole density in other studies [44,45].

IV. DISCUSSION

Table I provides a comparison of the selected transport parameters of undoped Ge/SiGe 2DHG between early reports in the literature and our study. As the mobility was in the ultrahigh region, the presence of noninteger filling factors was visible at low temperature, as shown in the studies of Lodari *et al.* [4] and Kong *et al.* [5]. As the mobility decreased to $\sim 5 \times 10^5$ cm^2 V^{-1} s^{-1}, the noninteger filling factors were absent in the studies of Sammak *et al.* [8] and Zhang *et al.* [9]. In contrast, the quantum states at plausible filling factors of $\nu = 5/2$ and $\nu = 3/2$ at 1.71 K with a maximum mobility of 5.2×10^5 cm^2 V^{-1} s^{-1} were observed in our study. Additionally, at the lower mobility of 2.1×10^5 cm^2 V^{-1} s^{-1}, Lodari *et al.* also observed the signatures of the $\nu = 5/3$ fractional state at a temperature of 1.7 K [10]. Thus, there is no unique relationship between the mobility and quantum Hall states at low temperature. The mobility is dominated by large-angle scattering from kinds of omnipresent residual impurities at different hole densities, whereas quantum scattering time τ_q is sensitive to both background scattering and remote scattering [13]. The quantum states at filling factors $\nu = 5/2$ and $\nu = 3/2$ of undoped Ge/SiGe could be closely correlated to the quantum scattering time τ_q by the single-particle level broadening of $\Gamma = \hbar/2\tau_q$. As shown in Table I, the quantum states at noninteger filling factors were observable when τ_q

TABLE I. Selected transport parameters of undoped Ge/SiGe 2DHG adopted from this study and early literatures.

Reference	Maximum mobility ($\times 10^5$ cm^2 V^{-1} s^{-1})	Maximum mobility scattering time (ps)	Quantum scattering time (ps)	Noninteger filling factors
This work	5.2	34	1.2–2.3	Yes
Kong *et al.* [5]	20	100	1.7	Yes
Lodari *et al.* (2022) [4]	10	N.A.	N.A.	Yes
Sammak *et al.* [8]	5.0	20	0.74	No
Zhang *et al.* [9]	4.6	13	0.5	No
Lodari *et al.* (2021) [10]	2.1	8.7	0.87	Yes

was no less than ∼0.87 ps, although the undoped Ge/SiGe heterostructures were grown and the Hall-bar devices were prepared by different academic research groups. Thus, a long τ_q directly reflected a narrow level broadening, and implied weak scattering caused by surrounding charged impurities. The reduced level broadening favors the improvement of coherence time in the spin manipulation of a quantum dot based qubit [10,40].

In our study, the density of remote charged impurities was much higher than the density of background charged impurities and $k_F h_{\text{eff}}$ was in between 3.3 and 4.3 at hole densities between 1.21×10^{11} and 2.40×10^{11} cm^{-2}. The total scattering could, therefore, be dominated by the remote charged impurities. No matter the Ge QW was prepared in an ultralow disorder level; in a realistic case the unavoidably introduced charged impurities at the interface between the as-grown heterostructure and the gate dielectric thin film during device processing dominantly contribute the total scattering to the Ge QW. Compared to the study of Kong *et al.* where a *similar heterostructure* was used [5], our study showed a relatively lower hole mobility (shorter mobility scattering time), but manifested comparable quantum scattering time and quantum Hall effects. The degraded mobility could be caused by edge roughness on the Ge channel in device processing, such as dry etching of a Hall-bar shaped mesa. The less compromised quantum scattering time could benefit from fewer remote charged impurities introduced during the whole device processing. It is ultimately essential to control the density of remote charged impurities to limit the overall scattering. For instance, the interface state density could be drastically reduced by inserting an ultrathin SiO_2 buffer layer between Al_2O_3 and Si [46,47]. The SiO_2 layer can be fabricated either by the *in situ* oxidation of the Si cap or by atomic layer deposition [47].

V. CONCLUSION

In conclusion, a degraded hole mobility of 5.2×10^5 cm^2 V^{-1} s^{-1} but a long quantum scattering time τ_q up to 2.3 ps were obtained in a processed undoped Ge/SiGe heterostructure. The heterostructure was grown using the reduced pressure chemical vapor deposition (RPCVD) method and the device fabrications were compatible with well-established semiconductor technology. In the study, not only integer quantum Hall effects (IQHEs) of filling factors down to $\nu = 1$, but also the quantum states of the filling factors between $\nu = 1$ and 2, and between $\nu = 2$ and 3 were observed at 1.71 K at low hole density. Although the mobility was degraded unavoidably due to the fabrication processes, the long quantum scattering time, indicating great quantum quality, was less compromised in this ultraclean and low-disordered undoped Ge/SiGe heterostructure. Thus, this study confirmed the mobility/quality dichotomy, and supported the heterostructure as an idea platform to obtain high-quality quantum electronic devices for exploring fundamental physics and building gate-controlled quantum dots.

ACKNOWLEDGMENTS

This research was funded by the National Natural Science Foundation of China (Grants No. 11974030 and No. 92165208), the Beijing Natural Science Foundation (Grant No. 1202010), the Innovation Program for Quantum Science and Technology (Project No. 2021ZD0302300), the National Key Research and Development Plan (Project No. 2016YFA0301701), and the Youth Innovation Promotion Association of CAS (Project No. 2020037). The device fabrications were done with the assistance of Peking Nanofab.

[1] G. Scappucci, C. Kloeffel, F. A. Zwanenburg, D. Loss, M. Myronov, J. J. Zhang, S. D. Franceschi, G. Katsaros, and M. Veldhorst, The germanium quantum information route, Nat. Rev. Mater **6**, 926 (2021).

[2] N. W. Hendrickx, W. I. L. Lawrie, M. Russ, F. van Riggelen, S. L. de Snoo, R. N. Schouten, A. Sammak, G. Scappucci, and M. Veldhorst, A four-qubit germanium quantum processor, Nature (London) **591**, 580 (2021).

[3] H. Watzinger, J. Kukučka, L. Vukušić, F. Gao, T. Wang, F. Schäffler, J. J. Zhang, and G. Katsaros, A germanium hole spin qubit, Nat. Commun. **9**, 3902 (2018).

[4] M. Lodari, O. Kong, M. Rendell, A. Tosato, A. Sammak, M. Veldhorst, A. R. Hamilton, and G. Scappucci, Lightly strained germanium quantum wells with hole mobility exceeding one million, Appl. Phys. Lett. **120**, 122104 (2022).

[5] Z. Kong, Z. Li, G. Cao, J. Su, Y. Zhang, J. Liu, J. Liu, Y. Ren, L. Wei, G. Guo, Y. Wu, H. H. Radamson, J. Li, Z. Wu, H. Li,

J. Yang, C. Zhao, and G. Wang, Undoped strained Ge quantum well with ultrahigh mobility of two million, ACS Appl. Mater. Interface. **15**, 28799 (2023).

[6] W. van dar Wel, E. G. Haanappal, J. E. Mooij, C. J. P. M. Harmans, J. P. Andre, G. Weimann, K. Ploog, C. T. Foxon, and J. J. Harris, Selection criteria for AlGaAs-GaAs heterostructures in view of their use as a quantum Hall resistance standard, J. Appl. Phys. **65**, 3487 (1989).

[7] M. J. Manfra, Molecular beam epitaxy of ultra-high-quality AlGaAs/GaAs heterostructures: Enabling physics in low-dimensional electronic systems, Annu. Rev. Condens. Matter Phys. **5**, 347 (2014).

[8] A. Sammak, D. Sabbagh, N. W. Hendrickx, M. Lodari, B. P. Wuetz, A. Tosato, L. Yeoh, M. Bollani, M. Virgilio, M. A. Schubert, P. Zaumseil, G. Capellini, M. Veldhorst, and G. Scappucci, Light effective hole mass in undoped Ge/SiGe quantum wells, Adv. Funct. Mater. **29**, 1807613 (2019).

[9] D. Zhang, J. Lu, Z. Liu, F. Wan, X. Liu, Y. Pang, Y. Zhu, B. Cheng, J. Zheng, Y. Zuo, and C. Xue, Sharp interface of undoped Ge/SiGe quantum well grown by ultrahigh vacuum chemical vapor deposition, Appl. Phys. Lett. **121**, 022102 (2022).

[10] M. Lodari, N. W. Hendrickx, W. I. L. Lawrie, T. K. Hsiao, L. M. K. Vandersypen, A. Sammak, M. Veldhorst, and G. Scappucci, Low percolation density and charge noise with holes in germanium, Mater. Quantum. Technol. **1**, 011002 (2021).

[11] S. Das Sarma and E. H. Hwang, Mobility versus quality in two-dimensional semiconductor structure, Phys. Rev. B **90**, 035425 (2014).

[12] M. Sammon, M. A. Zudov, and B. I. Shklovskii, Mobility and quantum mobility of modern GaAs/AlGaAs heterostructures, Phys. Rev. Mater **2**, 064604 (2018).

[13] B. Rössner, D. Chrastina, G. Isella, and H. von Känel, Scattering mechanisms in high-mobility strained Ge channels, Appl. Phys. Lett. **84**, 3058 (2004).

[14] M. Virgilio and G. Grosso, Type-I alignment and direct fundamental gap in SiGe based heterostructures, J. Phys. Condens. Matter **18**, 1021 (2006).

[15] N. W. Hendrickx, D. P. Franke, A. Sammak, M. Kouwenhoven, D. Sabbagh, L. Yeoh, R. Li, M. L. V. Tagliaferri, M. Virgilio, G. Capellini, G. Scappucci, and M. Veldhorst, Gate-controlled quantum dots and superconductivity in planar germanium, Nat. Commun. **9**, 2835 (2018).

[16] See Supplemental Material at http://link.aps.org/supplemental/10.1103/PhysRevB.108.045303 for detailed fabrication processes of Hall-bar field-effect device; calculation of hole density; extraction of percolation density; calculation of mean free path; extraction of effective mass and quantum scattering time; the density dependency and magnetic dependency of effective mass. It also contains Refs. [21,22,25–32].

[17] W. I. L. Lawrie, H. G. J. Eenink, N. W. Hendrickx, J. M. Boter, L. Petit, S. V. Amitonov, M. Lodari, B. Paquelet Wuetz, C. Volk, S. G. J. Philips, G. Droulers, N. Kalhor, F. van Riggelen, D. Brousse, A. Sammak, L. M. K. Vandersypen, G. Scappucci, and M. Veldhorst, Quantum dot arrays in silicon and germanium, Appl. Phys. Lett. **116**, 080501 (2020).

[18] M. A. Zudov, O. A. Mironov, Q. A. Ebner, P. D. Martin, Q. Shi, and D. R. Leadley, Observation of microwave-induced resistance oscillations in a high-mobility two-dimensional hole gas in a strained Ge/SiGe quantum well, Phys. Rev. B **89**, 125401 (2014).

[19] Q. Shi, Q. A. Ebner, and M. A. Zudov, Hall field-induced resistance oscillations in a *p*-type Ge/SiGe quantum well, Phys. Rev. B **90**, 161301(R) (2014).

[20] S. K. Shin, S. Huang, N. Fukata, and K. Ishibashi, Top-gated germanium nanowire quantum dots in a few-electron regime, Appl. Phys. Lett. **100**, 073103 (2012).

[21] L. A. Tracy, E. H. Hwang, K. Eng, G. A. Ten Eyck, E. P. Nordberg, K. Childs, M. S. Carroll, M. P. Lilly, and S. Das Sarma, Observation of percolation-induced two-dimensional metal-insulator transition in a Si MOSFET, Phys. Rev. B **79**, 235307 (2009).

[22] J. S. Kim, A. M. Tyryshkin, and S. A. Lyon, Annealing shallow Si/SiO_2 interface traps in electron-beam irradiated high-mobility metal-oxide-silicon transistors, Appl. Phys. Lett. **110**, 123505 (2017).

[23] D. Monroe, Y. H. Xie, E. A. Fitzgerald, P. J. Silverman, and G. P. Watson, Comparison of mobility-limiting mechanisms in high-mobility $Si_{1-x}Ge_x$ heterostructures, J. Vac. Sci. Technol. B **11**, 1731 (1993).

[24] J. Y. Li, C. T. Huang, L. P. Rokhinson, and J. C. Sturm, Extremely high electron mobility in isotopically-enriched ^{28}Si two-dimensional electron gases grown by chemical vapor deposition, Appl. Phys. Lett. **103**, 162105 (2013).

[25] D. Shoenberg, *Magnetic Oscillations in Metals* (Cambridge University Press, Cambridge, 1984).

[26] R. Winkler, Theory for the cyclotron resonance of holes in strained asymmetric Ge-SiGe quantum wells, Phys. Rev. B **53**, 10858 (1996).

[27] J. P. Eisenstein, H. L. Störmer, V. Narayanamurti, A. C. Gossard, and W. Wiegmann, Effect of Inversion Symmetry on the Band Structure of Semiconductor Heterostructures, Phys. Rev. Lett. **53**, 2579 (1984).

[28] B. Habib, E. Tutuc, S. Melinte, M. Shayegan, D. Wasserman, S. A. Lyon, and R. Winkler, Spin splitting in GaAs (100) two-dimensional holes, Phys. Rev. B **69**, 113311 (2004).

[29] D. Laroche, S. H. Huang, Y. Chuang, J. Y. Li, C. W. Liu, and T. M. Lu, Magneto-transport analysis of an ultra-low-density two-dimensional hole gas in an undoped strained Ge/SiGe heterostructure, Appl. Phys. Lett. **108**, 233504 (2016).

[30] B. Habib, M. Shayegan, and R. Winkler, Spin–orbit interaction and transport in GaAs two-dimensional holes, Semicond. Sci. Technol. **24**, 064002 (2009).

[31] B. A. Foreman, Analytic model for the valence-band structure of a strained quantum well, Phys. Rev. B **49**, 1757 (1994).

[32] B. Rößner, G. Isella, and H. von Känel, Effective mass in remotely doped Ge quantum wells, Appl. Phys. Lett. **82**, 754 (2003).

[33] L. A. Terrazos, E. Marcellina, Z. Wang, S. N. Coppersmith, M. Friesen, A. R. Hamilton, X. Hu, B. Koiller, A. L. Saraiva, D. Culcer, and R. B. Capaz, Theory of hole-spin qubits in strained germanium quantum dots, Phys. Rev. B **103**, 125201 (2021).

[34] M. Lodari, A. Tosato, D. Sabbagh, M. A. Schubert, G. Capellini, A. Sammak, M. Veldhorst, and G. Scappucci, Light effective hole mass in undoped Ge/SiGe quantum wells, Phys. Rev. B **100**, 041304(R) (2019).

[35] Q. Qian, J. Nakamura, S. Fallahi, G. C. Gardner, J. D. Watson, S. Lüscher, J. A. Folk, G. A. Csáthy, and M. J. Manfra, Quantum lifetime in ultrahigh quality GaAs quantum wells:

Relationship to $\Delta_{5/2}$ and impact of density fluctuations, Phys. Rev. B **96**, 035309 (2017).

[36] S. Huang, N. Fukata, M. Shimizu, T. Yamaguchi, T. Sekiguchi, and K. Ishibashi, Classical Coulomb blockade of a silicon nanowire dot, Appl. Phys. Lett. **92**, 213110 (2008).

[37] S. Huang, S. K. Shin, N. Fukata, and K. Ishibashi, A single-electron transistor and an even-odd effect in chemically synthesized Ge nanowires, J. Appl. Phys. **109**, 036101 (2011).

[38] X. Mi, T. M. Hazard, C. Payette, K. Wang, D. M. Zajac, J. V. Cady, and J. R. Petta, Magnetotransport studies of mobility limiting mechanisms in undoped Si/SiGe heterostructures, Phys. Rev. B **92**, 035304 (2015).

[39] D. Laroche, S. H. Huang, E. Nielsen, Y. Chuang, J. Y. Li, C. W. Liu, and T. M. Lu, Scattering mechanisms in shallow undoped Si/SiGe quantum wells, AIP Adv. **5**, 107106 (2015).

[40] I. L. Drichko, A. A. Dmitriev, V. A. Malysh, I. Yu. Smirnov, H. von Känel, M. Kummer, D. Chrastina, and G. Isella, Effective g factor of 2D holes in strained Ge quantum wells, J. Appl. Phys. **123**, 165703 (2018).

[41] Y. Jing, S. Huang, K. Zhang, J. Wu, Y. Guo, H. Peng, Z. Liu, and H. Q. Xu, Weak antilocalization and electron–electron interaction in coupled multiple-channel transport in a Bi_2Se_3 thin film, Nanoscale **8**, 1879 (2016).

[42] M. Meng, S. Huang, C. Tan, J. Wu, Y. Jing, H. Peng, and H. Q. Xu, Strong spin–orbit interaction and magnetotransport in semiconductor Bi_2O_2Se nanoplates, Nanoscale **10**, 2704 (2018).

[43] M. Failla, J. Keller, G. Scalari, C. Maissen, J. Faist, C. Reichl, W. Wegscheider, O. J. Newell, D. R. Leadley, M. Myronov, and J. Lloyd-Hughes, Terahertz quantum Hall effect for spin-split heavy-hole gases in strained Ge quantum wells, New J. Phys. **18**, 113036 (2016).

[44] Q. Shi, M. A. Zudov, C. Morrison, and M. Myronov, Strong transport anisotropy in Ge/SiGe quantum wells in tilted magnetic fields, Phys. Rev. B **91**, 201301(R) (2015).

[45] Q. Shi, M. A. Zudov, C. Morrison, and M. Myronov, Spinless composite fermions in an ultrahigh-quality strained Ge quantum well, Phys. Rev. B **91**, 241303(R) (2015).

[46] D. Kim, J. Y. Choi, S. W. Ryu, and W. B. Kim, Improved interface and electrical properties by inserting an ultrathin SiO_2 buffer layer in the Al_2O_3/Si heterojunction, Adv. Funct. Mater. **29**, 1807271 (2019).

[47] G. Dingemans, N. M. Terlinden, M. A. Verheijen, M. C. M. Van de Sanden, and W. M. M. Kessels, Controlling the fixed charge and passivation properties of Si(100)/Al_2O_3 interfaces using ultrathin SiO_2 interlayers synthesized by atomic layer deposition, J. Appl. Phys. **110**, 093715 (2011).